

# Convective heat transport in stratified atmospheres at low and high Mach number

Evan H. Anders and Benjamin P. Brown

Department of Astrophysical & Planetary Sciences, University of Colorado – Boulder and  
Laboratory for Atmospheric and Space Physics, Boulder, CO

Convection in astrophysical systems is stratified and often occurs at high Rayleigh number (Ra) and low Mach number (Ma). Here we study stratified convection in the context of plane-parallel, polytropically stratified atmospheres. We hold the density stratification ( $n_\rho$ ) and Prandtl number (Pr) constant while varying the superadiabaticity and Ra. We find that Ma is primarily controlled by the superadiabaticity of the atmosphere. We also examine the behavior of the Nusselt number (Nu), which quantifies the efficiency of convective heat transport, and the Reynolds number (Re), which quantifies how turbulent our solutions are.

## INTRODUCTION

Convection transports energy in stellar and planetary atmospheres. In these objects, flows are compressible and feel the atmospheric stratification. While in some systems this stratification is negligible, it is significant in regions such as the convective envelope of the Sun, which spans 14 density scale heights. In the bulk of these systems, flows are at very low Mach Number (Ma), but numerical constraint have restricted most studies of compressible convection to high Ma. These studies have provided important insight into the low temperature, high Ma region near the Sun’s surface, but few fundamental properties of low Ma convection which characterize deeper motions are known.

In the widely-studied Rayleigh-Bénard (RB) problem of Boussinesq convection, upflows and downflows are symmetrical and the conductive flux ( $\propto \nabla T$ ) approaches zero in the convective interior. Early numerical experiments of moderate-to-high Ma compressible convection in two [1–4] and three [5, 6] dimensions revealed that these two hallmark characteristics of RB convection change significantly when stratification is included. Downflow lanes become fast and narrow, and upflow lanes turn into broad, slow upwellings. Furthermore, the entropy gradient is negated by convection rather than the temperature gradient, and a significant conductive flux can exist in the presence of efficient convection.

In RB convection, there exist two primary dynamical control parameters: the Rayleigh number (Ra, the ratio of buoyant driving to diffusive damping) and the Prandtl number (Pr, the ratio of viscous to thermal diffusivity). These numbers control two useful measures of turbulence in the evolved solution: the Reynolds number (Re, the strength of advection to viscous diffusion) and the Peclet number (Pe = Re Pr). Stratified atmospheres with negative entropy gradients are unstable to convection. The magnitude of the unstable entropy gradient, or the superadiabaticity, joins Ra and Pr as an important control parameter. This *superadiabatic excess* [1],  $\epsilon$ , which sets the scale of the atmospheric entropy gradient, primarily controls the Ma of the evolved solution.

In this letter we study the behavior of convective heat transport, quantified by the Nusselt number (Nu), in plane-parallel, two-dimensional, polytropically stratified atmospheres. We vary  $\epsilon$  and Ra while holding Pr, aspect ratio, boundary conditions, and initial atmospheric stratification constant. We describe experimental methods in section II, including the construction of atmospheres, equations, and numerical methods. Results are described in section III and their implications are discussed in section IV.

## EXPERIMENT

We examine a monatomic ideal gas with an adiabatic index of  $\gamma = 5/3$  whose equation of state is  $P = R\rho T$ . This is consistent with the approach used in earlier work and is the simplest stratified extension of RB. We study atmospheres which are initially polytropically stratified,

$$\begin{aligned}\rho_0(z) &= \rho_t(1 + L_z - z)^m, \\ T_0(z) &= T_t(1 + L_z - z),\end{aligned}\quad (1)$$

where  $m$  is the polytropic index and  $L_z$  is the depth of the atmosphere. The height coordinate,  $z$ , increases upwards in the range  $[0, L_z]$ . We specify the depth of the atmosphere,  $L_z = e^{n_\rho/m} - 1$ , by choosing the number of density scale heights,  $n_\rho$ , it spans. Throughout this letter we set  $n_\rho = 3$ . Satisfying hydrostatic equilibrium sets the value of gravity,  $g = RT_t(m+1)$ , which is constant with depth. We study two-dimensional atmospheres with aspect ratios of 4 where the  $x$  coordinate has the range  $[0, 4L_z]$ .

Convective dynamics are controlled by the superadiabaticity of the atmospheres as well as the atmospheric diffusivities. The superadiabaticity, or the magnitude of the (negative) entropy gradient, is set by the superadiabatic excess,  $\epsilon = m_{ad} - m$ , where  $m_{ad} = (\gamma - 1)^{-1}$ . The atmospheric thermal diffusivity,  $\chi$ , and kinematic viscosity (or viscous diffusivity),  $\nu$ , are determined by the Rayleigh number (Ra) and the Prandtl number (Pr). We set  $\text{Pr} = \nu/\chi = 1$  throughout this work. The polytropic initial conditions are in thermal equilibrium,  $\kappa_0 \partial_z T_0 =$

const, so  $\kappa_0 = \chi\rho_0$  must be constant. To keep  $\text{Pr}$  constant with height, we set  $\chi = \chi_t/\rho_0$  and  $\nu = \nu_t/\rho_0$ . Under these constraints, the diffusivity profiles are specified by choosing  $\text{Ra}$  at the top of the domain,

$$\text{Ra}_{\text{top}} = \frac{gL_z^3(\Delta S_0/c_P)}{\nu_t \chi_t}, \quad (2)$$

where  $\Delta S_0 = \epsilon \ln z_0$  is the entropy difference between the top and bottom boundaries and  $c_P = R\gamma(\gamma - 1)^{-1}$  is the specific heat at constant pressure. The profiles of  $\nu$  and  $\chi$  are constant with time, and  $\text{Ra}$  at the bottom of the atmosphere is greater than  $\text{Ra}_{\text{top}}$  by a factor of  $e^{2n\rho}$ . This formulation leaves the thermal conductivity,  $\kappa = \rho\chi$ , and the dynamic viscosity,  $\mu = \rho\chi$ , free to evolve as the density profile changes.

We decompose our thermodynamic variables such that  $T = T_0 + T_1$  and  $\ln \rho = (\ln \rho)_0 + (\ln \rho)_1$ , and the velocity  $\mathbf{u} = u\hat{x} + w\hat{z}$  has no background component. We evolve the Fully Compressible Navier-Stokes equations,

$$\frac{\partial \ln \rho}{\partial t} + \nabla \cdot \mathbf{u} = -\mathbf{u} \cdot \nabla \ln \rho, \quad (3)$$

$$\frac{\partial \mathbf{u}}{\partial t} + \nabla T - \nu \nabla \cdot \bar{\boldsymbol{\sigma}} - \bar{\boldsymbol{\sigma}} \cdot \nabla \nu = -\mathbf{u} \cdot \nabla \mathbf{u} - T \nabla \ln \rho + \mathbf{g} + \nu \bar{\boldsymbol{\sigma}} \cdot \nabla \ln \rho, \quad (4)$$

$$\begin{aligned} \frac{\partial T}{\partial t} - \frac{1}{c_V} (\chi \nabla^2 T + \nabla T \cdot \nabla \chi) &= \\ -\mathbf{u} \cdot \nabla T - (\gamma - 1) T \nabla \cdot \mathbf{u} & \\ + \frac{1}{c_V} (\chi \nabla T \cdot \nabla \ln \rho + \nu [\bar{\boldsymbol{\sigma}} \cdot \nabla] \cdot \mathbf{u}), \end{aligned} \quad (5)$$

with the viscous stress tensor given by

$$\sigma_{ij} \equiv \left( \frac{\partial u_i}{\partial x_j} + \frac{\partial u_j}{\partial x_i} - \frac{2}{3} \delta_{ij} \nabla \cdot \mathbf{u} \right). \quad (6)$$

Taking an inner product of (4) with  $\mathbf{u}$  and adding it to (5) reveals the full energy equation,

$$\frac{\partial}{\partial t} \left( \rho \left[ \frac{|\mathbf{u}|^2}{2} + c_V T + \phi \right] \right) + \nabla \cdot (\mathbf{F}_{\text{conv}} + \mathbf{F}_{\text{cond}}) = 0, \quad (7)$$

where  $\mathbf{F}_{\text{conv}} \equiv \mathbf{F}_{\text{enth}} + \mathbf{F}_{\text{KE}} + \mathbf{F}_{\text{PE}} + \mathbf{F}_{\text{visc}}$  is the convective flux and  $\mathbf{F}_{\text{cond}} = -\kappa \nabla T$  is the conductive flux. The individual contributions to  $\mathbf{F}_{\text{conv}}$  are the enthalpy flux,  $\mathbf{F}_{\text{enth}} \equiv \rho u(c_V T + P/\rho)$ ; the kinetic energy flux,  $\mathbf{F}_{\text{KE}} \equiv \rho |\mathbf{u}|^2 \mathbf{u}/2$ ; the potential energy flux,  $\mathbf{F}_{\text{PE}} \equiv \rho \mathbf{u} \phi$  (with  $\phi \equiv -gz$ ); and the viscous flux,  $\mathbf{F}_{\text{visc}} \equiv -\rho \nu \mathbf{u} \cdot \bar{\boldsymbol{\sigma}}$ , and each must be considered. Understanding how these fluxes interact is crucial in characterizing convective heat transport.

We utilize the Dedalus<sup>1</sup> [7] pseudospectral framework to time-evolve (3)-(5) using an implicit-explicit (IMEX),

third-order, four-step Runge-Kutta timestepping scheme RK443 [8]. Variables are time-evolved on a dealiased Chebyshev (vertical) and Fourier (horizontal, periodic) domain in which the physical grid dimensions are  $3/2$  the size of the coefficient grid. Physical grid sizes range from 96x384 grid points at the lowest values of  $\text{Ra}$  to 1536x6144 grid points at  $\text{Ra}_{\text{top}} > 10^7$ . By using IMEX timestepping, we implicitly step the stiff linear acoustic wave contribution and are able to efficiently study flows at moderate ( $\approx 1$ ) and very low ( $\approx 10^{-4}$ )  $\text{Ma}$ . Our equations take the form of the FC equations in [9], extended to include  $\nu$  and  $\chi$  which vary with depth, and we follow the approach there. This IMEX approach has been successfully tested against a nonlinear benchmark of the compressible Kelvin-Helmholtz instability [10].

We impose impenetrable, stress free, fixed temperature boundary conditions at the top and bottom of the domain such that  $w = \partial_z u = T_1 = 0$  at  $z = \{0, L_z\}$ .  $T_1$  is initially filled with random white noise whose magnitude is infinitesimal compared to  $T_0$  and  $\epsilon$ . We filter this noise spectrum in coefficient space, such that 25% of the coefficients have power. We non-dimensionalize our computational domains by setting all thermodynamic variables to unity at  $z = L_z$  by choosing  $R = T_t = \rho_t = 1$ . By this choice, the non-dimensional grid length scale is the inverse temperature gradient scale and the simulation timescale is the isothermal sound crossing time,  $\tau_I$ , of this unit length. Meaningful convective dynamics occur on timescales of the atmospheric buoyancy time,  $t_b = \tau_I \sqrt{L_z/g\epsilon}$ , and all reported results are taken from time averages over many buoyancy times starting  $100t_b$  after the start of our simulations in order to assure our results are not biased by the convective transient.

## RESULTS

Solutions were time-evolved until a long time average of the fluxes showed little variance with depth. By performing a linear stability analysis, we determined that the onset of convection occurs at  $\text{Ra}_{\text{c,top}} = \{11.15, 10.06, 10.97, 10.97\}$  for  $\epsilon = \{1.0, 0.5, 10^{-4}, 10^{-7}\}$  respectively. We studied Rayleigh numbers from values at onset to values  $\geq 10^6 \text{Ra}_{\text{c,top}}$  for  $\epsilon = 0.5$ , up to roughly  $10^5 \text{Ra}_{\text{c,top}}$  at  $\epsilon = 10^{-4}$ , and up to  $10^3 \text{Ra}_{\text{c,top}}$  for  $\epsilon = \{1, 10^{-7}\}$ .

We find that the Mach number is a strong function of  $\epsilon$  and a weak function of  $\text{Ra}$ . When  $\text{Ma} < 1$ ,  $\text{Ma} \propto \epsilon^{1/2}$ , but this relation breaks down as the mean  $\text{Ma}$  approaches 1 and the flows become supersonic (see Fig. 1a). At low  $\text{Ra}$  ( $\text{Ra}_{\text{c,top}} \lesssim 10^4$ ),  $\text{Ma} \propto \text{Ra}^{1/4}$ . At high  $\epsilon$  ( $\epsilon = 0.5$ , this scaling breaks down near  $\text{Ra} = 10^4$  where the flows become primarily supersonic. The scaling of  $\text{Ra}^{1/4}$  appears to break down for  $\text{Ra} \gtrsim 10^5$  at  $\epsilon = 10^{-4}$ , but computational constraints made it restrictively difficult to converge many runs in this region of parameter

<sup>1</sup> <http://dedalus-project.org/>

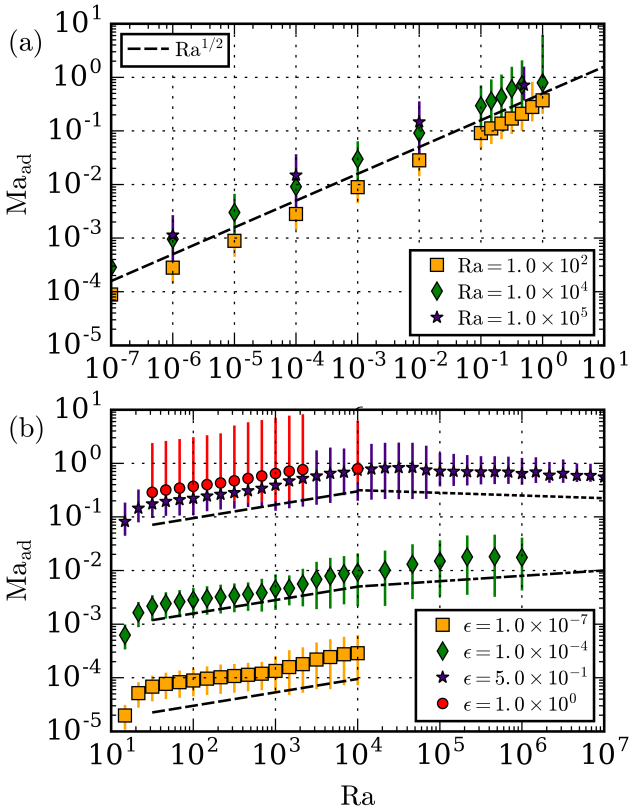


FIG. 1. The mean adiabatic Mach number of long-time-averaged profiles is shown. Error bars show the full range of  $Ma$  over the depth of the atmosphere. (a) When  $Ma < 1$  (below the black horizontal line),  $Ma \propto \epsilon^{1/2}$ . at low ( $10^2$ ) and moderate ( $10^5$ ) values of  $Ra$ . (b) When  $Ra$  is small,  $Ma \propto Ra^{1/2}$  (dashed lines). Once the mean  $Ma$  reaches 1 ( $\epsilon = \{0.5, 1\}$ ), this scaling breaks down and nearly all flows in the atmosphere are at  $Ma = 1$ . At low  $\epsilon$ , a consistent power law of  $Ma \propto Ra^{1/4}$  is retrieved.

space. Furthermore, the evolved thermodynamic variables,  $T_1/T_0, \rho_1/\rho_0 \propto \epsilon$ , are very small for low  $Ma$  flows, but are order 1 when  $\epsilon$  and  $Ma$  approach 1.

Low  $Ma$  flows ( $\epsilon = 10^{-4}$ ) display the classic narrow downflow and broad upflow lanes of stratified convection (Fig. 2a). While it has been suggested that pressure forces cause symmetry breaking in up- and downflows [3], at low  $\epsilon$  this effect seems to be secondary to flows obeying mass conservation as they traverse the stratified medium. Our choice of fixed-temperature boundary conditions allows the flux at the boundaries to vary, and runs at  $Ra > 10^4$  and  $\epsilon = 10^{-4}$  exhibit long-term states of flux disequilibrium. Roll solutions such as those pictured in Fig. 2a are punctuated by states of vigorous shearing, similar to those previously reported in two-dimensional RB convection [15]. During the roll states, the flux at the lower boundary exceeds that at the upper boundary and energy is stored in the system. During shearing states, convective transport is suppressed and  $Nu$  dimin-

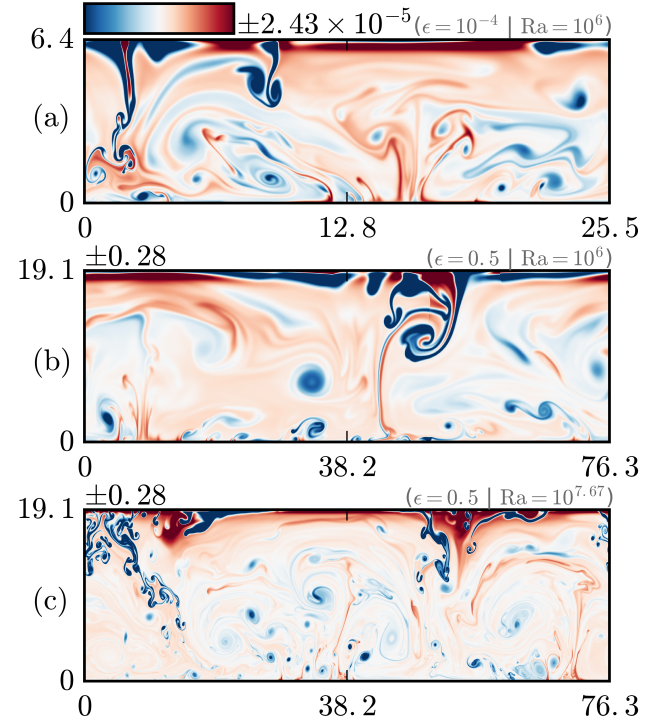


FIG. 2. Characteristic entropy fluctuations in evolved flows. The time- and horizontally-averaged profile is removed in all cases. (a) At high  $\epsilon$ , shock systems form near the upper downflow lanes ( $x \approx 45, z \approx 15-19$ ) at sufficiently high  $Ra$ . Shock-heated fluid then flows into the downflows as the shocks propagate across upflows. (b) At low  $\epsilon$  but at the same  $Ra$ , shock systems are absent, but otherwise the dynamics are similar. (c) As  $Ra$  is increased, downflows no longer span the entirety of the domain and individual small eddies are responsible for carrying the flux.

ishes while the flux at the upper boundary exceeds that at the lower boundary. Long term averages over both of these states produce flat flux profiles which can be sensibly analyzed.

At large  $Ma$  ( $\epsilon = 0.5$ ), bulk thermodynamic structures are similar but shock systems form in the upper atmosphere near downflow lanes once  $Ra$  is sufficiently large (Fig. 2b,c). Similar shock phenomena were reported in both two [4] and three [14] dimensional polytropic simulations previously. As  $Ra$  is increased to large values (Fig. 2c), thermodynamic structures no longer span the whole domain but rather break up into small eddies which traverse the domain multiple times before diffusing.

The efficiency of convection is quantified by the Nusselt number ( $Nu$ ).  $Nu$  is well-defined in RB convection as the total flux normalized by the steady-state conductive flux [11, 12]. In stratified convection  $Nu$  is more difficult to define, and we use a modified version of a traditional

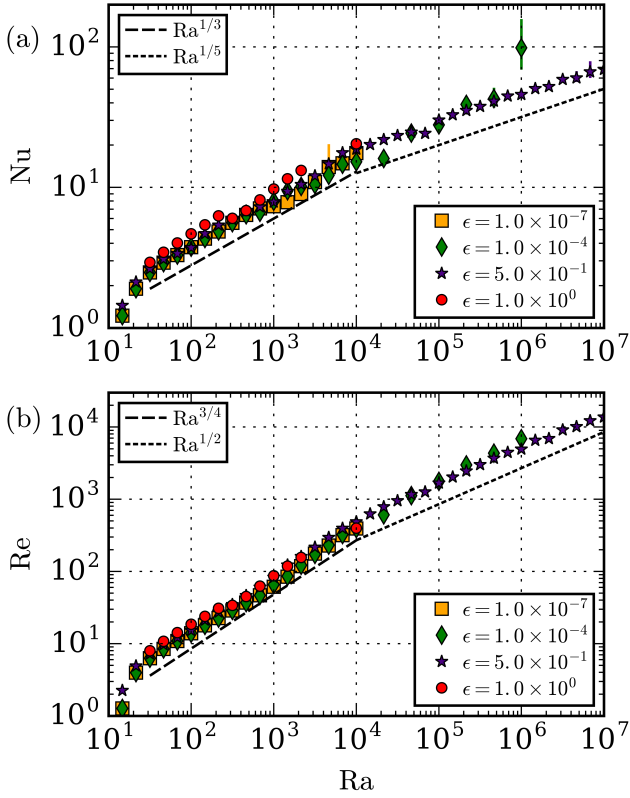


FIG. 3. Variation of Nu as Ra increases at high and low  $\epsilon$ . At high  $\epsilon$  (purple circles), a clear transition from the subsonic to supersonic regime is evident in the scaling of Nu with Ra at  $Ra_{top} \approx 10^4$ . In the low  $\epsilon$  regime (green diamonds and yellow squares), our observed Nu scalings collapse onto a similar line which is indistinguishable from a  $Ra_{top}^{2/7}$  scaling, as observed in RB convection [11]. Error bars are determined by the square root of the variance of the time-averaged Nu profile with depth and indicate whether or not a solution is well-converged. .

stratified Nusselt number [1, 3],

$$Nu \equiv \frac{\langle F_{conv,z} + F_{cond,z} - F_A \rangle}{\langle F_{cond,z} - F_A \rangle} = 1 + \frac{\langle F_{conv,z} \rangle}{\langle F_{cond,z} - F_A \rangle} \quad (8)$$

where  $F_{conv,z}$  and  $F_{cond,z}$  are the z-components of  $\mathbf{F}_{conv}$  and  $\mathbf{F}_{cond}$ , respectively and  $\langle \rangle$  are volume averages.  $F_A \equiv -\langle \kappa \rangle \partial_z T_{ad}$  is the conductive flux of the proper corresponding adiabatic atmosphere with  $\partial_z T_{ad} \equiv -g/c_P$  for an ideal gas in hydrostatic equilibrium. Here we specify  $\langle \kappa \rangle = \langle \rho \chi \rangle$ , which is nearly  $\kappa_0$  when  $\epsilon$  is small but can change appreciably for large values of  $\epsilon$ . In the Boussinesq approximation, under which  $\nabla S = 0$  only when  $\nabla T = 0$ , this definition reduces to the traditional definition of the Nusselt number [11, 12].

The variation of Nu with  $Ra_{top}$  is shown in Fig. 3a. At low to moderate  $Ra_{top}$ ,  $Nu \propto Ra_{top}^{1/3}$  regardless of  $\epsilon$  (NEED TO CITE A RB PAPER WITH A 1/3 POWER LAW [16] maybe?). At large  $Ra_{top}$ ,  $Nu \propto Ra_{top}^{1/5}$  at  $\epsilon = 0.5$ . The scaling of Nu with  $Ra_{top}$  is unclear at low  $\epsilon$  (so

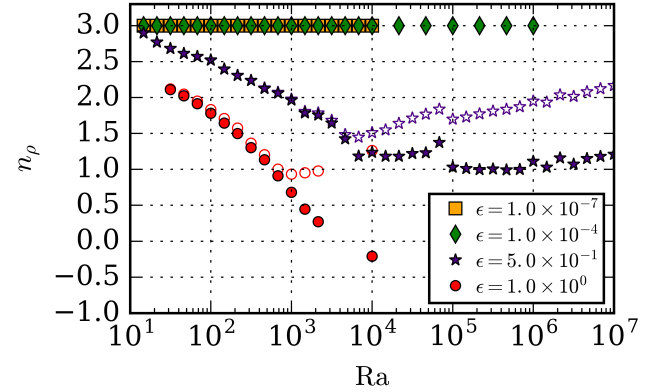


FIG. 4. We measure the stratification of evolved solutions in two ways. The solid symbols show  $\ln(\rho(0)/\rho(L_z))$ , or the density contrast as measured at the upper and lower boundary. The empty symbols show  $\ln(\max(\rho)/\min(\rho))$ . Unsurprisingly, at low  $\epsilon$  the evolved  $n_\rho$  is not different from the initial conditions to first order. At high  $\epsilon$ , the density contrast shrinks, and once the mean Ma approaches 1 the two methods of measuring the density stratification bifurcate as density inversions form within the thermal boundary layers.

I'll try to fill in that space with data from comps...time to fish it out of Lou and do post-processing hell).

The Reynolds number and Peclet number,

$$Re = \frac{|\mathbf{u}| L_z}{\nu}; \quad Pe = \text{Pr} Re, \quad (9)$$

quantify the importance of advection to diffusion in the evolved convective state. For  $\text{Pr} = 1$ , such as in this work,  $Pe = Re$ . Our choice of  $\{\nu, \chi\} \propto \rho_0^{-1}$  drastically changes the value of Re between the top and bottom of the atmosphere. We report values of Re at the midplane ( $z = L_z/2$ ) of the atmosphere in Fig. 3b. At low  $Ra_{top}$ ,  $Re \propto Ra_{top}^{3/4}$ , but at high  $Ra_{top}$  where the average Ma  $\approx 1$  for  $\epsilon = 0.5$ , this scaling gives way to a  $Re \propto Ra_{top}^{1/2}$ .

As the thermodynamic variables converge to their steady state values, the density profile evolves while remaining in hydrostatic equilibrium to zeroth order. In Fig. 4 we show the number of density scale heights present in the evolved solution using two measures. We find that once the average Ma of the domain becomes approximately one, large density inversions begin to form in the boundary layers, as was reported by [13]. The Regardless, the agreement of Nu across  $\epsilon$  despite the different effective stratifications felt in the simulations is striking.

## DISCUSSION

In this letter we have studied fundamental heat transport by stratified convection in simplified 2-D polytropic

atmospheres. We argue that these atmospheres are the natural extension of the RB problem to stratified systems, and are an ideal laboratory for understanding the basic properties of stratified convection.

At low Ra and Ma, the scaling of Nu with Ra is reminiscent of RB convection. However, at high Ra and Ma, the scaling breaks down to a  $\text{Ra}^{1/5}$  scaling unlike what is seen in Boussinesq convection. Similarly, the Reynolds number switches from a  $\text{Ra}^{3/4}$  to a  $\text{Ra}^{1/2}$  scaling in this regime shift. It is interesting that both of these scaling laws turn over by roughly a factor of 2/3.

Time-dependent oscillating shear states have developed spontaneously, as seen before in RB convection [15]. While computationally difficult, the highest values of Ra and the lowest value of  $\epsilon$  studied here are far from values found in nature. Future work will aim to better understand the mechanisms of shearing states and whether or not these states are attainable in three-dimensional, non-rotating atmospheres.

Furthermore, we have found that the stratification of these atmospheres evolves in a complex manner, and future work should aim to understand the importance of changing stratification on convective heat transport. Our studies here will serve as a foundation both for understanding and comparing heat transport in stratified convection to that in RB convection [11], and for future studies of transport in stratified convection. These results can be used to determine if simplified equation sets, such as the anelastic equations, carry heat in the same manner as the FC equations. This work will also be useful in coming to understand more realistic systems, such as rapidly rotating atmospheres [17], atmospheres bounded by stable regions [18], or regions with realistic profiles of  $\kappa$ .

### acknowledgements

EHA acknowledges the support of the University of Colorado's George Ellery Hale Graduate Student Fellowship. This work was additionally supported by NASA LWS grant number NNX16AC92G. Computations were conducted with support by the NASA High End Computing (HEC) Program through the NASA Advanced Supercomputing (NAS) Division at Ames Research Center

on Pleiades with allocations GID s1647 and GID g26133 (**AND ALSO THE NEW ONE AS OF 2017**). We thank Axel Brandenburg, Keith Julien, Mark Rast, and Jeff Oishi for many useful discussions.

- 
- [1] E. Graham, *Journal of Fluid Mechanics* **70**, 689 (1975).
  - [2] K. L. Chan, S. Sofia, and C. L. Wolff, *Astrophys. J.* **263**, 935 (1982).
  - [3] N. E. Hurlburt, J. Toomre, and J. M. Massaguer, *Astrophys. J.* **282**, 557 (1984).
  - [4] F. Cattaneo, N. E. Hurlburt, and J. Toomre, *ApJL* **349**, L63 (1990).
  - [5] F. Cattaneo, N. H. Brummell, J. Toomre, A. Malagoli, and N. E. Hurlburt, *Astrophys. J.* **370**, 282 (1991).
  - [6] N. H. Brummell, N. E. Hurlburt, and J. Toomre, *Astrophys. J.* **473**, 494 (1996).
  - [7] K. Burns, B. Brown, D. Lecoanet, J. Oishi, and G. Vasil, *Dedalus: Flexible framework for spectrally solving differential equations*, *Astrophysics Source Code Library* (2016), 1603.015.
  - [8] U. M. Ascher, S. J. Ruuth, and R. J. Spiteri, *Applied Numerical Mathematics* **25**, 151 (1997).
  - [9] D. Lecoanet, B. P. Brown, E. G. Zweibel, K. J. Burns, J. S. Oishi, and G. M. Vasil, *Ap. J.* **797**, 94 (2014), 1410.5424.
  - [10] D. Lecoanet, M. McCourt, E. Quataert, K. J. Burns, G. M. Vasil, J. S. Oishi, B. P. Brown, J. M. Stone, and R. M. O'Leary, *MNRAS* **455**, 4274 (2016), 1509.03630.
  - [11] H. Johnston and C. R. Doering, *Physical Review Letters* **102**, 064501 (2009), 0811.0401.
  - [12] J. Otero, R. W. Wittenberg, R. A. Worthing, and C. R. Doering, *Journal of Fluid Mechanics* **473**, 191 (2002).
  - [13] A. Brandenburg, K. L. Chan, Å. Nordlund, and R. F. Stein, *Astronomische Nachrichten* **326**, 681 (2005), astro-ph/0508404.
  - [14] A. Malagoli, F. Cattaneo, and N. H. Brummell, *ApJL* **361**, L33 (1990).
  - [15] D. Goluskin, H. Johnston, G. R. Flierl, and E. A. Spiegel, *Journal of Fluid Mechanics* **759**, 360 (2014).
  - [16] G. Ahlers, S. Grossmann, and D. Lohse, *Rev. Mod. Phys.* **81**, 503 (2009).
  - [17] K. Julien, E. Knobloch, A. M. Rubio, and G. M. Vasil, *Physical Review Letters* **109**, 254503 (2012).
  - [18] N. E. Hurlburt, J. Toomre, and J. M. Massaguer, *Astrophys. J.* **311**, 563 (1986).